Hindawi Publishing Corporation
International Journal of Microwave Science and Technology
Volume 2011, Article ID 468074, 9 pages
doi:10.1155/2011/468074

Research Article

Fully Distributed Tunable Bandpass Filter Based on $Ba_{0.5}Sr_{0.5}TiO_3$ Thin-Film Slow-Wave Structure

Sébastien L. Delprat,[1] JaeHo Oh,[1] Feng Xu,[2] Lin Li,[2] Erick E. Djoumessi,[2] Marwa Ismail,[1] Mohamed Chaker,[1] and Ke Wu[2]

[1] *INRS—Centre Énergie Materiaux Télécommunications, 1650 boulevard Lionel-Boulet, Varennes, QC, Canada J3X 1S2*
[2] *Poly-Grames Research Center École Polytechnique de Montréal, 2500 Chemin Polytechnique, Montréal, QC, Canada H3T 1J4*

Correspondence should be addressed to Sébastien L. Delprat, delprat@emt.inrs.ca

Received 13 April 2011; Accepted 15 June 2011

Academic Editor: Carlos Collado

This paper presents simulation and measurement results of fully distributed tunable coplanar bandpass filters (BPFs) with center frequencies around 6 GHz that make use of ferroelectric Barium Strontium Titanate ($Ba_xSr_{1-x}TiO_3$ or BST-x) thin film as tunable material. The two experimental bandpass filters tested are based on a novel frequency-agile structure composed of cascaded half wavelength slow-wave resonators (2 poles) and three coupled interdigital capacitors (IDCs) optimized for bias voltage application. Devices with gap dimensions of 10 and 3 μm are designed and fabricated with a two-step process on polycrystalline $Ba_{0.5}Sr_{0.5}TiO_3$ thin films deposited on alumina substrate. A frequency tunability of 9% is obtained for the 10 μm gap structure at $\pm$30 V with 7 dB insertion loss (the BST dielectric tunability being 26% with 0.04 loss tangent for this gap size). When the structure gap is reduced to 3 μm the center frequency shifts with a constant 9 dB insertion loss from 6.95 GHz at 0 V to 9.05 GHz at $\pm$30 V, thus yielding a filter tunability of 30% (the BST dielectric tunability being 60% with 0.04 loss tangent for this gap size), a performance comparable to some extent to localized or lumped element BPFs operating at microwave frequency (>2 GHz).

1. Introduction

The next generation of wireless networks such as reconfigurable and cognitive radio systems will require low-cost and highly integrated tunable microwave components that must handle room-temperature operations for multibands with wide tuning range, low power consumption, and small size. In particular, there is an increasing need for frequency-agile bandpass filters (BPFs) to replace large and costly filter banks used in the design of multiband microwave receivers [1]. In this context, significant efforts have been made since the last decade on the development of frequency-agile structures operating at microwave frequencies (above 2 GHz). Compared to semiconductor diodes [2] and RF microelectromechanical systems (MEMS) [3], ferroelectric-based devices present many advantages such as high power handling, continuous tuning, nanosecond switching speeds [4], and operation in a large frequency range with ease of fabrication and operation. Generally, the tuning is obtained by applying a bias voltage on the ferroelectric material and ferroelectric devices can be fully coplanar, very compact, and do not require hermetic packaging [5, 6].

Ferroelectric materials, in particular $Ba_xSr_{1-x}TiO_3$ (BST-x with x$\sim$0.5), present almost continuous dielectric constant tuning in the presence of an electric field and can be used for the design of BPFs either in a fully distributed architecture or a localized element approach. The main advantages of such a fully distributed architecture are related to a much more compact size of the devices (since the electrodes are laying on a material with a dielectric constant of 500–1000) and the simplicity of the fabrication process which involves only two steps (deposition of the ferroelectric material and electrode patterning). In the case of localized element devices, each ferroelectric varactor has to be either patterned on the substrate with deposition and etching processes or connected to the other parts of the circuit and these additional steps increase the fabrication costs. However, over the years, the localized elements have been preferred to

the fully distributed architecture for two main reasons: first because it is believed that localized elements will minimize the influence of the relatively high losses of BST in the GHz range ($\tan\delta \sim 0.05$) and also because it is more straightforward from the perspective of design simulation.

Moreover, some examples of ferroelectric-based bandpass filters (BPFs) with good performances have already been reported for the MHz region, all of them based on localized element BST varactors [7–9]. In the case of microwave frequency applications, performances in terms of frequency tunability and insertion loss are still not satisfactory. Again, most of the published papers concern BPFs utilizing localized element BST varactors [10–16] and only few are directly fabricated on BST layers [17–19]. In general, both circuit architectures suffer from high insertion losses and bandwidth variation with tuning as the tuning of resonance and inter-resonator coupling should be made in a synchronized way. The first ones generally present higher tuning capabilities at low voltages with better insertion losses: up to 22% at 30 V with 5.4 to 3.3 dB insertion loss for the state-of-the-art varactor-based BPF [14] compared to 7.7% at 150 V with 14.8 to 7.8 dB insertion loss for the best BST layer-based BPF [18]. However, varactor-based BPFs do not necessarily present better overall characteristics than fully distributed devices. The overall characteristics of a tunable filter can be represented by its figure of merit (FoM) as defined by Vendik's group [18]:

$$\text{FoM} = \frac{f_V - f_0}{\sqrt{\Delta f_V \cdot \Delta f_0}} \times \frac{1}{\sqrt{\text{IL}_V \cdot \text{IL}_0}} \left[\text{dB}^{-1}\right], \qquad (1)$$

where f_V and f_0 are the center resonant frequencies, Δf_V and Δf_0 are the -3 dB filter bandwidths, and IL_V and IL_0 are the insertion losses at the applied bias (V) and at 0 V, respectively.

For example, (1) yields to a comparable figure of merit for the two BPFs cited above (of 0.29 and 0.27 dB^{-1} resp.). It is also interesting to note that the rather large bias voltages used to tune a fully distributed architecture compared to the tuning of a localized element configuration is only a consequence of the gap sizes used to induce and adjust an electric field on the BST material (1.5 μm compared to 10 μm in the examples cited above). The performance limitations of BST layer-based tunable BPFs are mainly due to (i) the microwave characteristics of the BST layer; (ii) the filter design that is generally not optimized for the application of a bias voltage. Hence, before completely abandoning the fully distributed approach, it is important to study new filter design strategies adapted to the application of a bias voltage and make use of a ferroelectric material which possesses optimized microwave characteristics on low-cost material.

First of all, we have demonstrated in a previous work [20] that the dielectric tunability of polycrystalline BST-0.5 thin films deposited on alumina (Al_2O_3) substrates can be comparable to that obtained for epitaxial thin films grown on MgO, $LaAlO_3$ or Sapphire substrates. With a tight control on the BST-0.5 lattice parameter, it is possible to reach BST tunability as high as 25% at 3 V·μm^{-1} in the GHz range with a constant loss tangent ($\tan\delta$) of ~0.05. Secondly, we have recently developed new analytical methods in order to study the microwave characteristics of a novel design, called bilateral interdigital coplanar waveguide and its applications to tunable BPF design [21, 22]. This periodically loaded CPW structure was first introduced by Gorur et al. in 1998 [23], later used by Zhou et al. to design a passive bandpass filter [24] and by Yoon et al. for the conception of a tunable phase shifter [25]. This structure is particularly suitable for ferroelectric tunable device design since its fishbone shape is closely bordered by the ground planes, thus creating a constant gap all around the structure where a bias voltage can be easily applied. This slow-wave structure, hereafter called "Fishbone Filter" to simplify its complex name, also has the advantages to present a very compact size (λ_g is about 4 times shorter than conventional CPW line and can be further decreased with the use of BST) and it can be designed with the desired gap size in order to minimize the applied voltage necessary to tune the device.

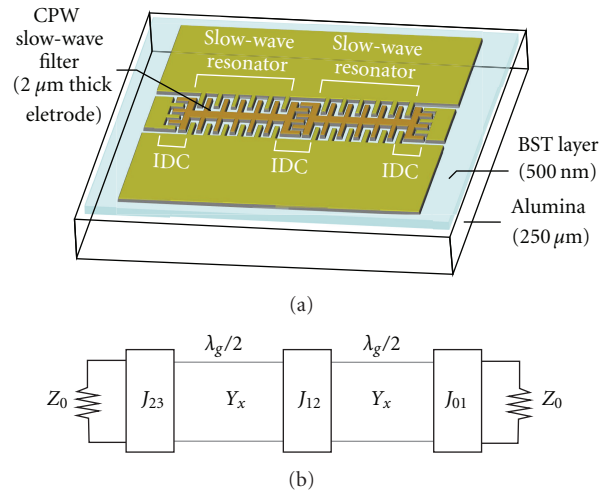

FIGURE 1: (a) Bilateral interdigital coplanar waveguide slow-wave filter (Fishbone Filter) structure on BST/Alumina substrate. (b) Equivalent network of the 2-pole BPF.

2. Filter Design and Fabrication

2.1. Filter Design. The first challenge for the design of Fishbone filters is that the analysis of a 2-pole bandpass filter like the one presented in Figure 1(a) is not straightforward. This is because there is a strong coupling between the interdigital capacitors (IDCs) and the slow-wave CPW line resonators. Accurate simulation of such BPFs requires direct full-wave analysis that should account for electrical and structural parameters. These simulations are time consuming, considering the very high dielectric constant of the BST layer, the complexity of the design, and the mesh size required for simulations. As a first approximation, one can use a numerical method in order to extract the parameters of the IDCs and the periodically loaded slow-wave line resonator structure and determine their geometry for a particular center frequency.

The complex capacitances of IDCs can be obtained by a conformal mapping method (CMM), using the following expression:

$$C = C_3 + C_n + C_{\text{end}}, \tag{2}$$

where n is the number of fingers of the IDC, C_3 and C_n are partial capacitances associated with groups of three and n fingers, respectively, and C_{end} is the end-to-end finger capacitance. Each partial capacitance is expressed as the product of known factors, depending only on the geometry of the IDC. Detailed calculation can be found in [26].

For the slow-wave line section, a finite difference frequency domain (FDFD) method was developed to extract the capacitance and conductance of the structure [22]. The FDFD method is used to solve partial differential equations of the slow-wave transmission line by considering it as a periodic guided-wave structure and base the calculation on a single period structure model. By using the discrete Maxwell's equations and incorporating the boundary conditions, one can obtain a matrix equation related to all electromagnetic fields on the meshes of a single period structure. First, in order to define the problem, it is necessary to rearrange the matrix equation, that is, all components related to the complex propagation constant γ should be put to the right side while other components are left on the left side of the equation. The complex propagation constant ($\gamma = \alpha + j\beta$) of the line is then the solution of a nonsymmetric generalized eigenvalue problem of the form

$$\mathbf{A}x = \gamma \mathbf{B}x, \tag{3}$$

where $\mathbf{A}$ denotes a large spare $n \times n$ matrix with eigenvalues $\lambda_1, \lambda_2, \ldots, \lambda_n$ and $\mathbf{B}$ represents the matrix composed by the desired eigenvalues, associated with the complex propagation constant γ. These matrices are related to the periodic model of the guided-wave structure and x is the electromagnetic vector. With the help of a shift-and-invert (SI) Arnoldi technique, one can get the eigenvalues of interest (γ) quickly and accurately. By comparing the propagation constant extracted with that of a normal CPW transmission line, the capacitance per unit length of the periodically loaded CPW line can be expressed as

$$C_I = \frac{1}{2} C_0 \left[\left(\frac{\beta_I}{\beta_0} \right)^2 - 1 \right], \tag{4}$$

where β_0 is the unloaded CPW line propagation constant, and β_I is the periodically loaded CPW line propagation constant.

The interdigital CPW slow-wave line conductance per unit length can be expressed as

$$G_I = \alpha_I \sqrt{\frac{(C_0 + 2C_I)}{L_0}}, \tag{5}$$

where α_I is the interdigital CPW line attenuation constant which can be also calculated by FDFD method.

The extracted capacitances and conductances (that only depend on geometrical dimensions) are then used to analyze the admittance inverters J_{01}, J_{12} and J_{23} of the equivalent network shown on Figure 1(b) in order to build a 2-pole Chebyshev-type bandpass filter made of cascaded half-wavelength slow-wave line resonators and coupled IDCs. Detailed description of the method used can be found in [22]. A further optimization of the design geometry is done by using IE3D package of Zeland Inc., a commercial full-wave simulation software.

Table 1: BST-0.5 thin film dielectric properties extracted from IDC and CPW scattering parameters measured between 1 and 13 GHz. The reported BST dielectric tunability is measured at 3 GHz and 30 V applied bias.

Gap width	ε_r (at 3 GHz)	$\tan\delta$ (at 3 GHz)	BST Tunability (at 3 GHz and 30 V)
10 μm	980 ± 50	0.04 ± 0.005	26%
3 μm	1050 ± 50	0.04 ± 0.005	60%

Typical dielectric properties of the BST-0.5 thin films (ε_r and $\tan\delta$) used in these calculations are extracted from IDCs and CPW measurements at GHz frequencies by using a conformal mapping method (CMM) combined with a partial capacitance technique, as described in [27] (values presented in Table 1).

This approach was used to design two different Fishbone BPFs with a center frequency of ~6 GHz for the purpose of comparison; one with 10 μm gap and the other with 3 μm gap.

(i) On the first design (10 μm gap Fishbone BPF, as shown in Figure 2(a)) the first and last coupling IDCs are identical and their dimensions are given as follows: finger width (w) = 10 μm, gap between the fingers (s) = 10 μm, number and length of fingers are (N) = 19 and (L) = 155 μm, respectively. The dimensions of the middle coupling IDC are as follows: w = 10 μm, s = 10 μm, N = 20, and L = 50 μm. The two slow-wave resonators are 0.7 mm long and periodically loaded with 2 × 18 pairs of 10 μm width, 190 μm long fingers spaced by 10 μm. The total size of the filter is 2 × 0.42 mm.

(ii) The other design with a reduced gap width of 3 μm is shown in Figure 2(b). The dimensions of the first and last coupling IDCs are listed as follows: w = 11 μm, s = 3 μm, N = 9, and L = 155 μm. The middle coupling IDC dimensions are w = 11 μm, s = 3 μm, N = 10, and L = 47 μm. The two slow-wave resonators are 0.8 mm long and periodically loaded with 2 × 29 pairs of 11 μm width, 47 μm long fingers spaced by 3 μm. The total size of the filter is 2.1 × 0.12 mm.

For both designs, two independent DC-bias circuits consisting of quarter-wavelength line and stub connected to a bias pad (as can be seen in Figures 4 and 6) are used for tuning each pole of the filter.

2.2. Device Fabrication. $Ba_{0.5}Sr_{0.5}TiO_3$ (BST-0.5) thin films are deposited on 250 μm thick ceramic alumina (Al_2O_3)

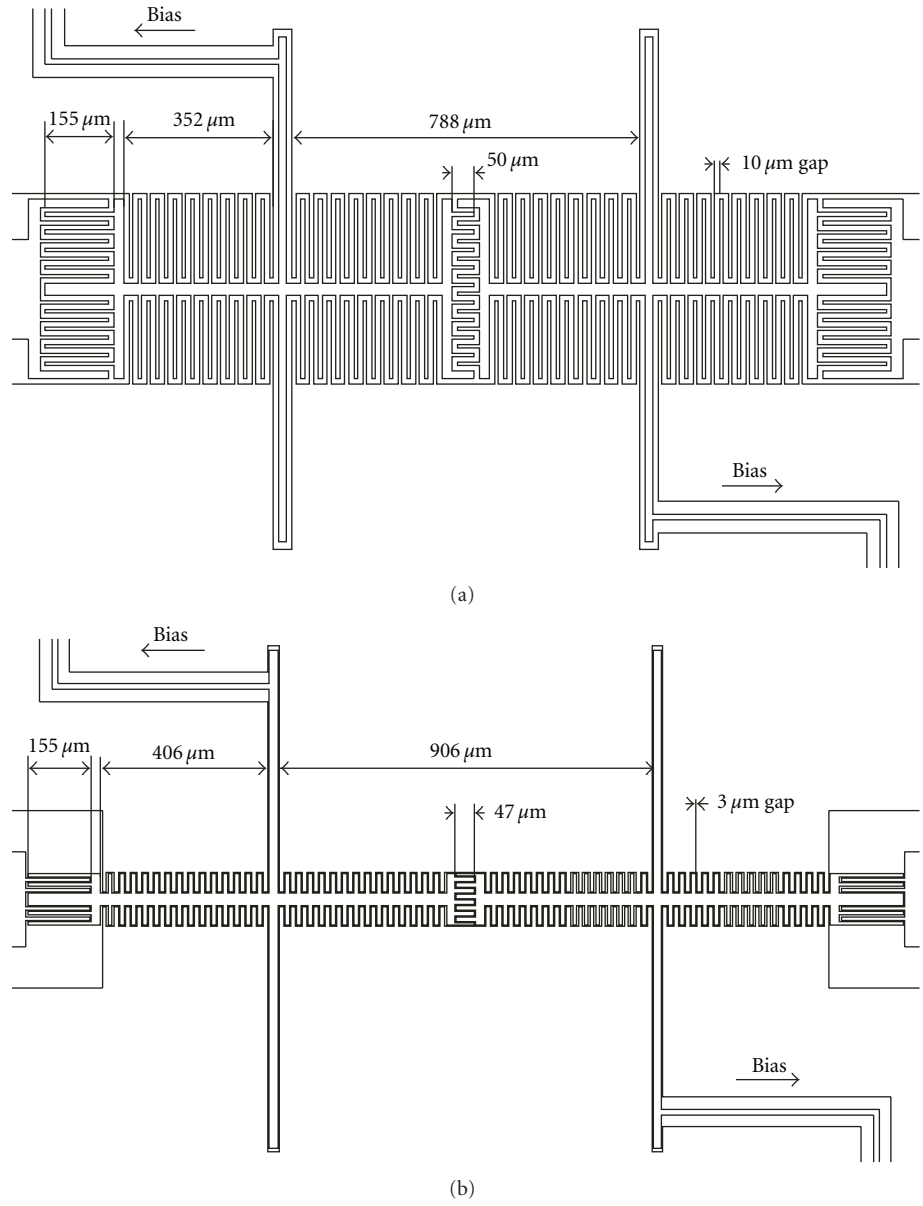

Figure 2: Layout of Fishbone bandpass filters with detailed dimensions of (a) 10 μm gap and (b) 3 μm gap Fishbone BPF.

substrate by mean of pulsed laser deposition (PLD). BST thin films with a thickness of 500 nm are prepared under vacuum and at 450°C using a KrF laser beam (1 J/cm^2) focused on a 99.9% pure BST-0.5 target. A final annealing in a furnace at 1050°C in oxygen for 3 hours is used to enhance the crystallinity of the film. The X-ray diffraction (XRD) spectrum of the obtained BST-0.5 thin film is shown in Figure 3. This XRD $\theta/2\theta$ spectrum shows that the film is polycrystalline with a lattice parameter of 3.950 Å, very close to bulk value ($a_{\text{bulk}} = 3.94946$ Å). For the CPW fabrication, single layer lift-off process with 7 μm thick SPR220 resist is used in order to obtain 2 μm thick electrodes. The electrode is composed of three e-beam evaporated layers: Ti (50 nm), Cu (1.9 μm), and Au (50 nm). Both Fishbone BPFs (10 and 3 μm gaps) are fabricated on the same $1'' \times 1''$ alumina substrate together with a TRL calibration kit and IDCs with 10 and 3 μm gaps used for the measurement of BST characteristics.

3. Results and Discussion

Tunable Fishbone BPF characteristics are measured on a HP 8510C vector network analyzer using a cascade Microtech probe station with 40A GSG Picoprobes. S parameters measurements are performed between 1 GHz and 13 GHz after calibration done on a TRL kit directly patterned on the BST/Alumina substrate.

Table 1 shows the extracted dielectric constant, loss tangent ($\tan\delta$), and tunability of the BST-0.5 thin film at 30 V extracted from the measured S parameters of both IDCs

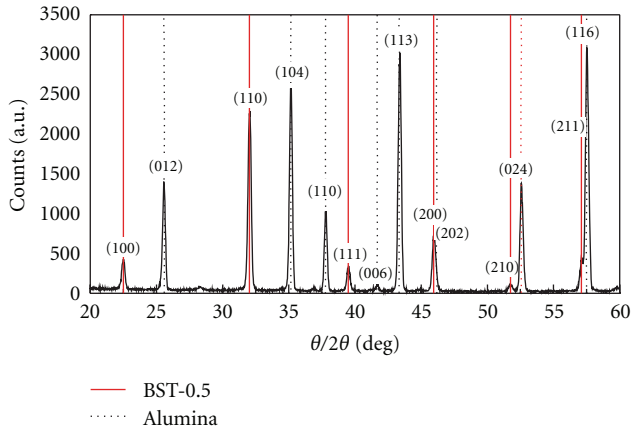

FIGURE 3: XRD spectra of BST-0.5 thin films deposited on polycrystalline Al_2O_3 (alumina) substrate.

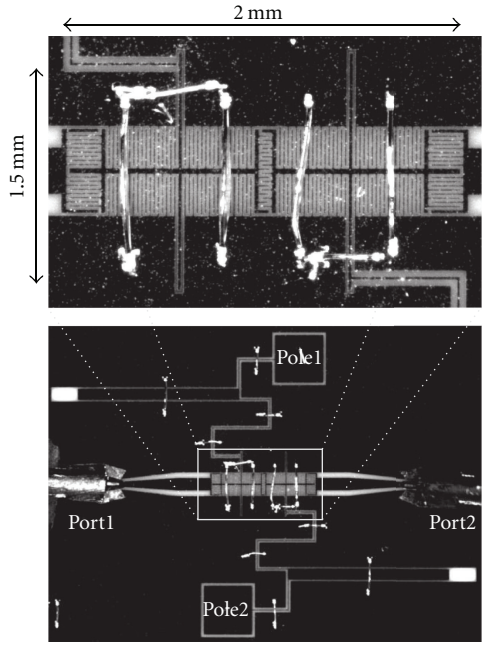

FIGURE 4: Picture of the fabricated 10 μm gap Fishbone bandpass filter under test.

and CPW measurements. The dielectric tunability for a given electric field being defined as

$$\Phi(V) = \frac{\varepsilon_r(0) - \varepsilon_r(V)}{\varepsilon_r(0)} \times 100\ [\%], \tag{6}$$

where $\varepsilon_r(0)$ and $\varepsilon_r(V)$ represent the dielectric constant at 0 V and at the applied DC bias V, respectively.

The measured dielectric constant of the 500 nm BST-0.5 layer is about 1000 with a loss tangent of 0.04 (error bars on these measurements, coming from the accuracy of the measured S parameters and the values of the film thickness and gap size used in the extraction model, are about 10%, which explains the discrepancy between the two different gap measurements). These microwave characteristics of $\varepsilon_r = 1000$ and $\tan\delta = 0.04$ are comparable to the ones reported by other groups in the GHz range [28, 29].

The measured BST tunabilities at 30 V and 3 GHz are 26% for the 10 μm gap IDC and 60% for the 3 μm gap IDC. This dielectric tunability improvement is consistent with the material response to the applied electric field (at constant 30 V bias) that increases from 3 V·μm^{-1} to 10 V·μm^{-1} as the IDC gap in decreased from 10 to 3 μm.

For the polarization of the designed Fishbone bandpass filters, two independent DC bias of up to −30 V and +30 V are applied on each pole of the BPF (denoted by pole 1 and pole 2). For the BPF tuning measurement, −/+ polarizations are preferred to the +/+ or −/− configuration in order to induce a polarization to the middle coupling capacitor. The filter tunability is defined as

$$F(V) = \frac{[f_V - f_0]}{f_0} \times 100\ [\%], \tag{7}$$

where f_V and f_0, the center frequencies at −V/+V and 0 V/0 V, respectively, are extracted from S_{21} characteristics.

3.1. Fishbone Bandpass Filter with 10 μm Gap. Figure 4 shows pictures of the 10 μm gap Fishbone BPF fabricated on BST-0.5. One can see that the electrodes are well defined and that some wire bridges are bonded where the ground planes are cut to avoid artifacts on the measurements. Figure 5 shows measured S_{11} and S_{21} parameters of the filter at 0 V/0 V and +30 V/−30 V polarizations. This figure indicates that by applying a ±30 V polarization, the resonant frequency shifts from 6.3 to 6.9 GHz, thus giving a filter tunability of 9% with insertion losses and filter bandwidth (at −3 dB) that are almost constant as the polarization voltage is increased: they go from −6 dB and 17.9% at 0 V to −6.3 dB and 15.1% at ±30 V. Return losses are better than −12 dB. The figure also provides the IE3D simulation results of the filter for corresponding BST characteristics ($\varepsilon_r = 1000$ and $\varepsilon_r = 750$ with $\tan\delta = 0.04$). A good agreement is obtained between simulated and measured S parameters.

3.2. Fishbone Bandpass Filter with 3 μm Gap. Pictures of the fabricated 3 μm gap Fishbone filter are shown in Figure 6, its simulated and measured responses are shown in Figure 7. At 0 V, the filter has a center frequency of 6.95 GHz with 23% bandwidth, −8.4 dB insertion loss and −12 dB return loss. At ±30 V the frequency is shifted by 30% to 9.05 GHz with a 15.8% bandwidth, −9.4 dB insertion loss, and −30 dB return loss. Simulated response (obtained by IE3D simulation) shows slightly better characteristics with a 42% frequency shift (from 6.2 GHz for $\varepsilon_r = 1000$ to 8.8 GHz for $\varepsilon_r = 400$) and 15 to 16% bandwidth. These differences are certainly coming from a small dimension tolerance of the patterned electrodes since it is a challenge to fabricate a constant 3 μm gap all along the structure with a 2 μm thick electrode and that the electrode sidewall is not perfectly straight. In that case, small gap differences or small defects are expected to cause differences in the filter response. It is also possible that the bias circuits (that are not taken into account in the simulations) induce a parasitic signal on the filter response

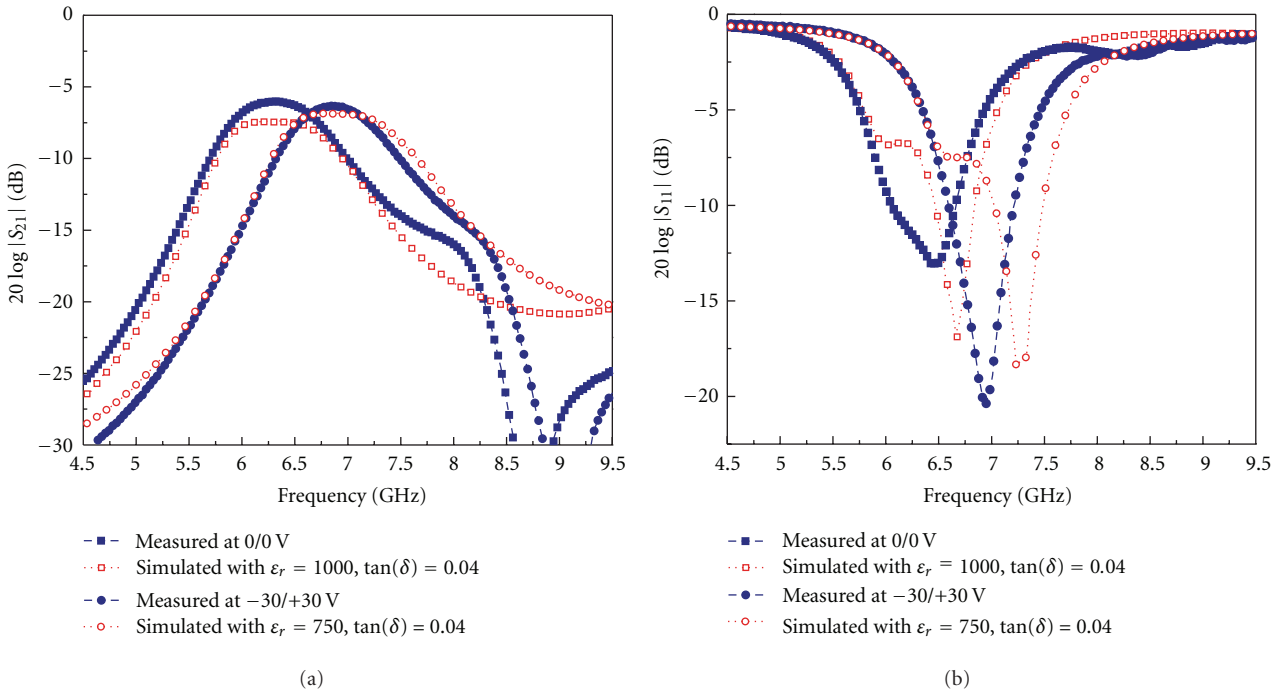

Figure 5: Measured and simulated S-parameters of the 10 μm gap bandpass filter without bias voltage and with a 30 V polarization applied on each pole (corresponding to BST dielectric constant of 1000 and 750, resp., with dielectric loss of 0.04 for the values used in the full-wave simulations).

Table 2: Comparison of the tested Fishbone filters with other microwave ferroelectric bandpass filters operating at room temperature (localized-element architecture on [10–16] and fully distributed architecture below [17–19]).

Ref.	f_0 (GHz)	Bias (V)	E(V·μm^{-1})	Frequency tunability	Bandwidth @ −3 dB (%)	Insertion loss (dB)	Q factor	FoM (dB^{-1})	FoM per kV bias
[10]	2.44	200	40	18%	24.6–31.3	5.1–3.3	10	0.14	0.7
[11]	8.35	30	20	6%	7.8–7.8	5.7–3.5	33	0.16	5.6
[12]	10.04	20	13.3	7.4%	19.9–23.2	2.9–1.95	**20**	**0.14**	**7.0**
[13]	8.75	100	20	25.3%	19.4–15.5	4–8	12	0.23	2.3
	11.7	100	20	22.2%	12–14	6–10	14	0.20	2.0
[14]	11.5	30	20	21.7%	15.7–15.9	5.4–3.3	**17**	**0.29**	**9.9**
[15]	19.86	400	8	9.1%	3.5–3.2	3.5–3.5	89	0.73	1.8
[16]	29	30	20	17.2%	15.5–15.5	6.9–2.5	**17**	**0.23**	**7.8**
[17]	2.7	200	8	29.6%	9.3–8.6	25.7–14.3	13	0.15	0.8
[18]	4.4	150	15	7.7%	2.6–2.4	14.8–7.8	57	0.27	1.8
[19]	16.68	100	4	2.9%	7.6–9.5	8.1–5.25	23	0.05	0.5
This work	6.3	30	3	9%	17.9–15.1	6–6.3	12	0.08	2.4
	6.95	30	10	30.2%	23.3–15.8	8.4–9.4	**8**	**0.15**	**5.2**

around 9 GHz that affects its performances, this has to be confirmed by other experiments.

Both designs show a slight increase of insertion losses as the filter is tuned. This increase is consistent with the simulated responses (that considers the loss tangent of the film to be constant) and may be attributed to the change in impedance matching of the structure as the dielectric constant of the films is reduced.

To the best of our knowledge the 30% tuning characteristics measured at 30 V for the 3 μm gap Fishbone filter is the best reported to date for a fully distributed microwave tunable BPF operating at room temperature. As can be seen in Table 2, that presents the characteristics of room temperature microwave tunable bandpass filters reported in the literature [10–19], previous higher tunability for a BST layer-based filter was presented by Su et al. [17] with

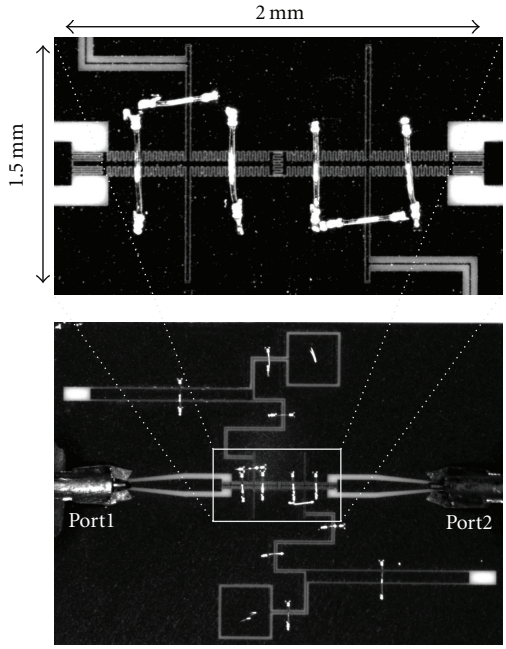

Figure 6: Picture of the fabricated 3 μm gap Fishbone bandpass filter under test.

a 29% tunability at 200 V but with insertion losses varying from −25.7 dB to −14.3 dB. In our case, a small variation of the filter bandwidth and insertion losses, as the center frequency is tuned, makes its characteristics comparable to some extent to the best varactor-based devices. The last column of the Table 2 presents the FoM per applied kV of bias, which represents a tradeoff between the overall characteristics of the tunable filter (FoM from equation (1)) and the DC bias used to reach it. This parameter is 5.2 $dB^{-1}\cdot kV^{-1}$ for the reported 3 μm gap Fishbone filter and 7 to 10 $dB^{-1}\cdot kV^{-1}$ for the three best varactor-based filters (all of them using varactors with 1.5 μm gap size). The only weakness of the Fishbone BPFs is its relatively low quality factor (Q) compared to other devices. This low Q is believed to come mainly from a relatively high loss tangent ($\tan\delta$) of the BST film and a poor impedance matching between the coupling capacitor and the transmission line at each end of the filter, which were designed on the basis of the 10 μm design to ease the test procedure. It is believed that with a better matching impedance of the circuit and lower losses of the BST layer (that can be achieve for example through codoping of the material [30]), the insertion losses of the filter can be significantly improved. Improvement of the analytical simulation models is also a key point in order to reach this goal.

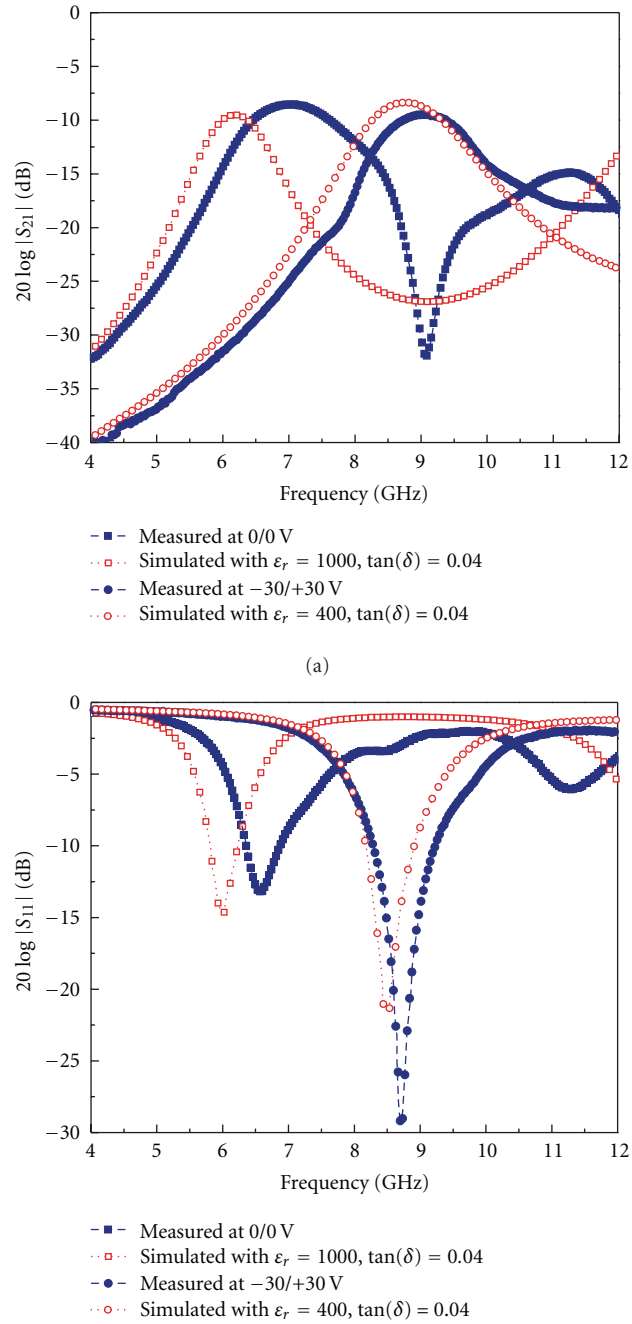

Figure 7: Measured and simulated S parameters of the 3 μm gap bandpass filter without bias voltage and with a 30 V polarization applied on each pole (corresponding to BST dielectric constant of 1000 and 400, resp., with dielectric loss of 0.04 for the values used in the full-wave simulations).

4. Conclusion

Two C-band tunable bandpass filters using a novel slow-wave structure and BST-0.5 layer deposited on Alumina substrate have been designed and characterized. Both filters show almost constant bandwidth and insertion loss and large tunability for low bias level. They exhibit a frequency tuning going from 9% at 30 V for the first design to up to 30% at 30 V for the second design. Improvement of the filter tunability is obtained by reducing the polarized gap surrounding the structure from 10 μm to 3 μm. Modification of the filter geometry is done through numerical simulations

and full-wave analysis of a 2-pole filter, resulting in a design that is only 2.1×0.12 mm in size for a 6.95 GHz center frequency. This study shows that the development of new CPW designs, optimized for the application of a bias voltage can make fully distributed BST-based devices attractive for practical applications, in particular "systems-on-a-chip" circuits, due to their very compact size and fabrication processes that are really simple compared to their localized element counterparts.

Acknowledgments

The authors would like to thank FCAR and NSERC for their financial support.

References

[1] J. Uher and W. J. R. Hoefer, "Tunable microwave and millimeter-wave band-pass filters," *IEEE Transactions on Microwave Theory and Techniques*, vol. 39, no. 4, pp. 643–653, 1991.

[2] S. R. Chandler, I. C. Hunter, and J. G. Gardiner, "Active varactor tunable bandpass filter," *IEEE Microwave and Guided Wave Letters*, vol. 3, no. 3, pp. 70–71, 1993.

[3] J. Brank, J. Yao, M. Eberly, A. Malczewski, K. Varian, and C. Goldsmith, "RF MEMS-based tunable filters," *International Journal of RF and Microwave Computer-Aided Engineering*, vol. 11, no. 5, pp. 276–284, 2001.

[4] A. B. Kozyrev, V. N. Osadchy, D. M. Kosmin, A. V. Tumarkin, T. Kaydanova, and D. Ginley, "Time tuning of ferroelectric film varactors under pulse voltages," *Applied Physics Letters*, vol. 91, no. 2, Article ID 022905, 2007.

[5] E. Marsan, J. Gauthier, M. Chaker, and K. Wu, "Tunable microwave device: status and perspective," in *Proceedings of the 3rd International IEEE Northeast Workshop on Circuits and Systems Conference, (NEWCAS '05)*, pp. 279–282, Quebec, Canada, June 2005.

[6] M. J. Lancaster, J. Powell, and A. Porch, "Thin-film ferroelectric microwave devices," *Superconductor Science and Technology*, vol. 11, no. 11, pp. 1323–1334, 1998.

[7] A. Tombak, J.-P. Maria, F. T. Ayguavives et al., "Voltage-controlled RF filters employing thin-film barium-strontium-titanate tunable capacitors," *IEEE Transactions on Microwave Theory and Techniques*, vol. 51, no. 2, pp. 462–467, 2003.

[8] M. T. Nguyen, W. D. Yan, and E. P. Horne, "Broadband tunable filters using high Q passive tunable ICs," in *Proceedings of the IEEE MTT-S International Microwave Symposium Digest*, pp. 951–954, Atlanta, Ga, USA, June 2008.

[9] G. Sanderson, A. H. Cardona, T. C. Watson et al., "Tunable if filter using thin-film BST varactors," in *Proceedings of the IEEE MTT-S International Microwave Symposium*, pp. 679–682, Honolulu, Hawaii, USA, June 2007.

[10] J. Nath, D. Ghosh, J. P. Maria et al., "An electronically tunable microstrip bandpass filter using thin-film Barium-Strontium-Titanate (BST) varactors," *IEEE Transactions on Microwave Theory and Techniques*, vol. 53, no. 9, pp. 2707–2712, 2005.

[11] S. Courreges, Y. Li, Z. Zhao, K. Choi, A. Hunt, and J. Papapolymerou, "A low loss X-band quasi-elliptic ferroelectric tunable filter," *IEEE Microwave and Wireless Components Letters*, vol. 19, no. 4, pp. 203–205, 2009.

[12] S. Courreges, Y. Li, Z. Zhao, K. Choi, A. T. Hunt, and J. Papapolymerou, "Two-pole X-band-tunable ferroelectric filters with tunable center frequency, fractional bandwidth, and return loss," *IEEE Transactions on Microwave Theory and Techniques*, vol. 57, no. 12, Article ID 5339095, pp. 2872–2881, 2009.

[13] J. Sigman, C. D. Nordquist, P. G. Clem, G. M. Kraus, and P. S. Finnegan, "Voltage-controlled Ku-band and X-band tunable combline filters using barium-strontium-titanate," *IEEE Microwave and Wireless Components Letters*, vol. 18, no. 9, pp. 593–595, 2008.

[14] J. Papapolymerou, C. Lugo, Z. Zhiyong, X. Wang, and A. Hunt, "A miniature low-loss slow-wave tunable ferroelectric BandPass filter from 11–14 GHz," in *Proceedings of the IEEE MTT-S International Microwave Symposium Digest*, pp. 556–559, San Francisco, Calif, USA, June 2006.

[15] V. N. Keis, A. B. Kozyrev, M. L. Khazov, J. Sok, and J. S. Lee, "20 GHz tunable filter based on ferroelectric (Ba,Sr)TiO3 film varactors," *Electronics Letters*, vol. 34, no. 11, pp. 1107–1109, 1998.

[16] S. Courreges, Y. Li, Z. Zhao et al., "A Ka-band electronically tunable ferroelectric filter," *IEEE Microwave and Wireless Components Letters*, vol. 19, no. 6, pp. 356–358, 2009.

[17] H. T. Su, P. M. Suherman, T. J. Jackson, F. Huang, and M. J. Lancaster, "Novel tunable bandpass filter realized using barium-strontium-titanate thin films," *IEEE Transactions on Microwave Theory and Techniques*, vol. 56, no. 11, Article ID 4657392, pp. 2468–2473, 2008.

[18] V. Pleskachev and I. Vendik, "Tunable microwave filters based on ferroelectric capacitors," in *Proceedings of the 15th International Conference on Microwaves, Radar and Wireless Communications, (MIKON '04)*, vol. 3, pp. 1039–1043, May 2004.

[19] G. Subramanyam, N. Mohsina, A. Al Zaman et al., "Ferroelectric thin-film based electrically tunable Ku-band coplanar waveguide components," in *Proceedings of the IEEE-MTT-S International Microwave Symposium Digest*, pp. 471–474, May 2001.

[20] S. L. Delprat, C. Durand, J. H. Oh, M. Chaker, and K. Wu, "Correlation between the lattice parameter and the dielectric tunability in nonepitaxial $Ba_{0.5}Sr_{0.5}$ Ti O_3 thin films," *Applied Physics Letters*, vol. 91, no. 6, Article ID 063513, 3 pages, 2007.

[21] N. Li, F. Xu, K. Wu, S. L. Delprat, and M. Chaker, "Slow-wave line filter design using full-wave circuit model of interdigital capacitor," in *Proceedings of the 35th European Microwave Conference*, vol. 1, pp. 409–412, October 2005.

[22] F. Xu, N. Li, K. Wu, S. Delprat, and M. Chaker, "Parameter extraction of interdigital slow-wave coplanar waveguide circuits using finite difference frequency domain algorithm," *International Journal of RF and Microwave Computer-Aided Engineering*, vol. 18, no. 3, pp. 250–259, 2008.

[23] A. Gorur, C. Karpuz, and M. Alkan, "Characteristics of periodically loaded CPW structures," *IEEE Microwave and Guided Wave Letters*, vol. 8, no. 8, pp. 278–280, 1998.

[24] J. Zhou, D. Hung, M. J. Lancaster, H. T. Su, and X. Xiong, "A novel superconducting CPW slow-wave bandpass filter," *Microwave and Optical Technology Letters*, vol. 34, no. 4, pp. 255–259, 2002.

[25] H. Yoon, K. J. Vinoy, and V. K. Varadan, "Design and development of micromachined bilateral interdigital coplanar waveguide RF phase shifter compatible with lateral double diffused metal oxide semiconductor voltage controller on silicon," *Smart Materials and Structures*, vol. 12, no. 5, pp. 769–775, 2003.

[26] E. Carlsson and S. Gevorgian, "Conformal mapping of the field and charge distributions in multilayered substrate

CPWs," *IEEE Transactions on Microwave Theory and Techniques*, vol. 47, no. 8, pp. 1544–1553, 1999.

[27] M. Ouaddari, S. Delprat, F. Vidal, M. Chaker, and K. Wu, "Microwave characterization of ferroelectric thin-film materials," *IEEE Transactions on Microwave Theory and Techniques*, vol. 53, no. 4, pp. 1390–1397, 2005.

[28] P. M. Suherman, T. J. Jackson, Y. Y. Tse et al., "Microwave properties of Ba0.5Sr0.5TiO3 thin film coplanar phase shifters," *Journal of Applied Physics*, vol. 99, no. 10, Article ID 104101, 7 pages, 2006.

[29] W. Chang, L. M. B. Alldredge, S. W. Kirchoefer, and J. M. Pond, "Device loss of (Ba,Sr)TiO3 film-based capacitors at 1–20 GHz," *Journal of Applied Physics*, vol. 105, no. 3, Article ID 034115, 8 pages, 2009.

[30] J. H. Oh, S. Delprat, M. Ismail, E. E. Djoumessi, M. Chaker, and K. Wu, "Improvement of Ba0.5Sr0.5TiO3 thin films microwave properties using codoping with Mg-W and Al-W," *Integrated Ferroelectrics*, vol. 112, no. 1, pp. 24–32, 2009.